General Disclaimer

One or more of the Following Statements may affect this Document

- This document has been reproduced from the best copy furnished by the organizational source. It is being released in the interest of making available as much information as possible.

- This document may contain data, which exceeds the sheet parameters. It was furnished in this condition by the organizational source and is the best copy available.

- This document may contain tone-on-tone or color graphs, charts and/or pictures, which have been reproduced in black and white.

- This document is paginated as submitted by the original source.

- Portions of this document are not fully legible due to the historical nature of some of the material. However, it is the best reproduction available from the original submission.

NASA Technical Memorandum 78524

Crustal Evolution Inferred from Apollo Magnetic Measurements

Palmer Dyal, William D. Daily, and Leonid L. Vanyan

September 1978

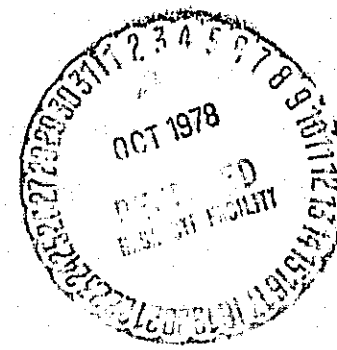

National Aeronautics and
Space Administration

NASA Technical Memorandum 78524

Crustal Evolution Inferred from Apollo Magnetic Measurements

Palmer Dyal, Ames Research Center, Moffett Field, California
William D. Daily, Eyring Research Institute, Provo, Utah
Leonid L. Vanyan, Space Research Institute, Academy of Sciences, Moscow, U.S.S.R.

National Aeronautics and
Space Administration

Ames Research Center
Moffett Field, California 94035

INTRODUCTION

In this paper we examine the topology of lunar remanent magnetic fields by analyzing simultaneous magnetometer and solar wind spectrometer data. The results of this study are then used to infer characteristics of the magnetized sources and their evolution during crustal formation.

Remanent magnetic fields were first measured on the moon by the Apollo 12 magnetometer in Oceanus Procellarum (Dyal et al., 1970). Subsequently, many additional surface and orbital experiments have measured fields over a large part of the lunar surface. Following these discoveries many investigators examined the interaction between lunar remanent fields and the solar wind plasma. Barnes et al. (1971) were the first to use this phenomena and estimate the remanent magnetic field scale size at the Apollo 12 landing site. They assumed that the field associated with the regions of permanent magnetization (magcons) were compressed by the solar wind flow. They also modeled the interaction mechanism at the lunar limb to explain magnetic perturbations in lunar orbital data reported by Sonett and Mihalov (1972).

Very early examination of simultaneous Apollo 12 magnetic and plasma data revealed a strong correlation between the plasma density and surface magnetic field changes (Dyal et al., 1972). Comparison of simultaneous interplanetary (OGO-5) and lunar surface (Apollo 12) plasma velocity data by Neugebauer et al. (1972), demonstrated that the solar wind was decelerated $\sim$ 50 km/sec as a result of its interaction with lunar remanent fields. In addition, the interaction near the limb resulted in occasional detection of the solar wind plasma as far as 18^{o} past the terminator. They modeled the interaction as a balance of plasma and magnetic field pressure normal to the lunar surface. Siscoe and Goldstein (1973) developed two pressure balance models for the field-plasma interaction.

In one case the source dipole axis is perpendicular to the surface and deflection currents close above the moon. In the other case the source dipole axis is parallel to the surface and the currents intersect the moon. Clay et al. (1975) studied several properties of the solar wind at the lunar surface from measurements obtained by the Apollo 12 and 15 solar wind spectrometers. In addition to plasma deceleration and deflection they measured heating of the protons in excess of adiabatic compressional heating and an increased level of fluctuations at frequencies above 3×10^{-5} Hz.

Vanyan (1977) has recently developed a diffusion model to describe the field-plasma interaction at the lunar surface and compared the model to a limited data set from one Apollo site. We will extend the diffusion theory in this paper to describe the interaction with fields characterized by two scale lengths and compare this model with data from three Apollo landing sites with crustal fields of very different intensity and topology. For the first time we compare local remanent field properties from this analysis with high spatial resolution magnetic maps recently obtained from the electron reflection experiment (Lin, private communication). We then consider these surface and orbital experimental results of the crustal magnetic fields along with the natural magnetic remanence measured in returned samples to postulate sources for the magnetizing field and the physical conditions in the crust during this evolutionary period.

MAGNETIC FIELD-SOLAR PLASMA DIFFUSION THEORY

In this section we discuss a field-plasma interaction model developed by Vanyan (1977) in which the local magnetic fields propagate into the solar plasma by means of diffusion. Interaction of the solar wind with global planetary magnetic fields, as in the case of the earth, is by a balance of plasma dynamic and magnetic pressure. The magnetic pressure, $B^2/8\pi$, of the

local remanent fields at each of the Apollo 12, 14, and 16 landing sites is larger than the nominal solar wind dynamic pressure (approximately 4×10^{-9} dynes/cm^2). However, solar wind spectrometer data from the Apollo landing sites indicate that the solar plasma impinges directly on the lunar surface with small changes from interplanetary values of its density or bulk velocity (Clay et al., 1975; Neugebauer et al., 1972). Therefore, it is clear that scale sizes of the local fields are too small for the dynamic pressure of the solar wind to significantly distort the field by a pressure balance mechanism. Barnes et al. (1971) calculated that the interaction region for the plasma-field pressure balance interaction has a theoretical scale length $L_o \sim 10$ km. If the local field scale length is $L \gg L_o$ the particles experience significant momentum change during the interaction and a shock may form. When $L \ll L_o$ the interaction is weak or nonexistent since the field scale size is smaller than the electron gyroradius or electron inertial length and little momentum change is imparted to the particles in the interaction. For the intermediate case of $L \sim L_o$ we will model the interaction using the theory of Vanyan (1977) which does not require a balance of magnetic and plasma pressure.

To model the field diffusion into the plasma we consider the magnetic field of a magnetized layer, the top of which is at a depth d below the lunar surface. Magnetization M in the layer is proportional to $2a \cos mz$ where $m = 2\pi/L$ and L is the scale size characteristic of the magnetization (see Figure 1). We use the Apollo coordinate system which has its origin on the lunar surface at the landing site. The x axis is directed radially outward from the surface; the y and z axes are tangential to the surface, directed eastward and northward respectively. The magnetic field in the nonconducting lunar half space $x < 0$ satisfies Maxwell's equation $\nabla \times \mathbf{B} = (4\pi/c)\mathbf{j} = 0$ which becomes Laplace's equation $\nabla^2 \mathbf{B} = 0$ with the solution

Fig.

$$B_x = (ae^{-m(d+x)} + be^{mx})\cos mz \qquad (1)$$

where c is the velocity of light and $\underset{\sim}{j}$ is the current. In the plasma the field is given by $\nabla \times \underset{\sim}{E} = -(1/c)\,\partial\underset{\sim}{B}/\partial t$ and Ohm's law $\underset{\sim}{j} = \sigma\underset{\sim}{E}$ which together yield the diffusion equation

$$\frac{\partial \underset{\sim}{B}}{\partial t} = \frac{c^2}{4\pi\sigma}\nabla^2\underset{\sim}{B} \qquad (2)$$

where $\underset{\sim}{E}$ is the electric field. The electrical conductivity of a collisionless plasma is $\sigma = ine^2/(m\omega)$ where the electron density, charge, and mass are n, e, and m respectively and ω is the frequency (see Jackson, 1962). Diffusion of the field into the plasma is by a transverse electromagnetic wave propagating along the x axis $\underset{\sim}{B} = \underset{\sim}{B}_o e^{-\beta x}\, e^{i\alpha x - i\omega t}$, where the propagation constant is $k = \alpha + i\beta$. For these conditions equation (2) becomes

$$\nabla^2\underset{\sim}{B} = \delta^2\underset{\sim}{B} \qquad (3)$$

with $\delta^2 = \omega_p{}^2/c^2$ ($\omega_p{}^2 = 4\pi ne^2/m$, the plasma frequency). For $\omega < \omega_p$, k becomes purely imaginary, and the wave does not propagate in the plasma but decays with a length of δ^{-1}. Solution to equation (3) in the limit as $\omega \to 0$ is $B_{x,z} = ce^{-qx}\cos mz$ where $q^2 = m^2 + \delta^2$. From the magnetic boundary conditions at the lunar surface it can be shown that the distorted and undistorted lunar field $\underset{\sim}{B}$ and $\underset{\sim}{B}_R$ respectively are related by

$$B_x - B_{Rx} = -\frac{q-m}{q+m}B_{Rx} \equiv -f(n,L)B_{Rx} \qquad (4)$$

for the radial component and

$$B_z - B_{Rz} = \frac{q-m}{q+m}B_{Rz} \equiv f(n,L)B_{Rz} \qquad (5)$$

for the tangential component. Note that for the more general case with two field components tangent to the surface equation (5) is valid, the total tangential fields replacing the z components. The theory is linear so that the

sum of two solutions is also a solution. We will use superposition of solutions to model the interaction data with magnetization characterized by two different scale sizes.

The undistorted remanent field $\underset{\sim}{B}_R$ at each Apollo site is measured when the moon is in the geomagnetic tail and thereby shielded from the solar plasma The distorted field is calculated from the difference in the field measured at the surface by an Apollo surface magnetometer and the field measured in lunar orbit by the Explorer 35 magnetometer or the Apollo subsatellite magnetometer. This difference is $\underset{\sim}{B} = \underset{\sim}{B}_A - \underset{\sim}{B}_E = \underset{\sim}{B}_p + \underset{\sim}{B}_R + \underset{\sim}{B}_D$ where $\underset{\sim}{B}_A$ is the field measured at the surface and $\underset{\sim}{B}_E$ is the field external to the moon measured by a lunar orbiting magnetometer. The undistorted remanent field is $\underset{\sim}{B}_R$ and the interaction field from currents in the plasma is $\underset{\sim}{B}_D$. Fluctuations in the external field $\underset{\sim}{B}_E$ induce eddy currents in the moon. The poloidal field associated with these currents oppose the change in the external field. This poloidal induction mode dominates magnetization, toroidal, and diamagnetic modes when the moon is in the solar wind. However, in the limit of low-frequency driving field fluctuations, the poloidal induction vanishes. Therefore in the analysis we use one hour averaged data in which we estimate the residual poloidal fields to be $\lesssim$ 10% of the external field. Furthermore, since the induced fields $\underset{\sim}{B}_p$ have dipolar symmetry about the direction of the external field change, and not about the remanent field, poloidal contributions will tend to reduce the correlation in the data predicted by equations 4 and 5 without biasing the analysis.

ANALYSIS OF LUNAR SURFACE MAGNETIC AND PLASMA DATA

Measurements used in this analysis were obtained from several different lunar surface and orbital instruments: Apollo 12, 15, and 16 lunar surface magnetometers, Apollo 14 and 16 lunar portable magnetometers, Lunokhod 2

magnetometer, Apollo 12 and 15 solar wind spectrometers, Explorer 35 magnetometer and the Apollo 15 and 16 subsatellite magnetometers. The network of three lunar surface magnetometers were deployed by astronauts on the Apollo 12, 15, and 16 missions. The vector magnetic field was measured 3 times per second with 0.2 gamma resolution and transmitted to earth from each of these Apollo sites. A detailed description of these instruments is reported by Dyal and Gordon (1973). The lunar portable magnetomers were developed for deployment and operation during the astronaut traverses on the Apollo 14 and 16 missions. A total of six vector field measurements were obtained of surface remanent fields. The Lunokhod 2 magnetometer was deployed in LeMonnier Bay and obtained vector field measurements during a traverse of several kilometers in this region. A more detailed description of this experiment is given by Dolginov et al. (1976). The solar wind density and vector velocity measurements were obtained at the Apollo 12 and 15 lunar surface sites by the Solar Wind Spectrometer which has been described by Clay et al. (1972). These instruments measure plasma spectra every 28 seconds and continuously transmit the data to earth. The magnetic fields in the near lunar environment were measured by the orbiting Explorer 35 and Apollo 15 and 16 subsatellite magnetometers. The Explorer 35 instrument, orbiting the moon every 11.5 hours with aposelene of 9390 km and periselene of 2570 km, measured the vector components every 6.14 seconds with a resolution of 0.4 gamma. A more detailed description of this experiment is reported by Sonett et al. (1967). The Apollo 15 and 16 subsatellite magnetometers orbited approximately 100 km above the lunar surface with a 2 hour period and measured the vector field components every 2 seconds with a resolution of 0.2 gamma. The subsatellite magnetometer characteristics are described in detail by Coleman et al. (1972).

The lunar crustal magnetic fields have been measured at four Apollo landing sites, one Lunokhod 2 site, and mapped by the Apollo subsatellite.

The source for these permanent magnetic fields is the remanence in the lunar crustal material. This remanence has been measured in representative lunar samples from all landing sites and is generally considered to be due to free iron (e.g., Strangway et al., 1973; Nagata, 1972; Runcorn et al., 1970). The geologic and remanent field characteristics are different at each of the three Apollo sites studied in this paper. The Apollo 12 instrument was deployed on the eastern edge of Oceanus Procellarum, a mare region north of Mare Cognetum and southeast of Lansberg crater. The site coordinates are 3.2°S and 23.4°W and the remanent field magnitude is 38 ± 2 gammas. The Apollo 15 instrument was deployed on a mare plain near the eastern edge of Mare Imbrian at coordinates 26.1°N and 3.7°E. The measured remanent field was only 3.4 ± 2.9 gamma and directed mostly vertical. The Apollo 16 instrument was deployed in lunar highlands at the western edge of the Descartes Mountains near part of the highest topographic features on the near side of the Moon. The remanent field was measured at five different locations along the astronaut traverse. The largest field of 327 ± 7 gammas was measured near Smoky Mountain while the remanent field at the stationary magnetometer is 234 ± 3 gammas. The Apollo 16 magnetometer is at coordinates 8.9°S and 15.5°E.

Magnetic field, plasma density, and plasma velocity measurements for a five day period from Apollo 12 are shown in Figure 2. This data was obtained during the first lunar orbit after the Apollo 12 landing when the moon was in the magnetosheath for two days and in the free streaming solar wind for three days. There is a correlation of more than 0.8 between the change in remanent field component tangential to the lunar surface and solar wind particle density, as predicted by the diffusion interaction model. On the other hand, there is a correlation of only - 0.22 between distortion of the remanent field and solar wind velocity. The simultaneous increase in tangential field distortion and velocity during the last hours of day 330 is coincidental because of the

density enhancement associated with the leading edge of the solar wind high velocity stream. After passage of the leading edge and its density enhancement, the slow rise in velocity beginning on day 332 does not result in the tangential field increase expected by the pressure balance mechanism. A similar lack of correlation is found between hour averages of solar wind velcity and field distortion in the remainder of the data we have examined. It is also significant that the solar plasma changes the remanent field more than 15 gammas which is 50% of the unperturbed 28 gamma steady field. This is one of the largest time dependent lunar magnetic signals measured at the surface.

The Apollo 15 magnetic field and simultaneous plasma data are shown in Figure 3 for a five day time period when the moon was in the magnetosheath and the free streaming solar wind. The components of the steady field are small at this site: $B_{Rx} = + 3.3 \pm 1.5\ \gamma$, $B_{Ry} = + 0.9 \pm 2.0\ \gamma$, and $B_{Rz} = - 0.2 \pm 1.5\ \gamma$. It is apparent from this figure that there is very little correlation between any of the field and plasma parameters. We expect the interaction at this location to be negligible since Equations (4) and (5) predict no field change in the limit as $B_{OR} \to 0$.

Fig. 3

Figure 4 shows five days of Apollo 16 magnetic and solar wind plasma data. The remanent field at this site was larger than that measured at any other Apollo site: $B_{Rx} = - 181 \pm 3\ \gamma$, $B_{Ry} = - 57 \pm 3\ \gamma$, and $B_{Rz} = + 136 \pm 2\ \gamma$. There is an obvious correlation between the Apollo surface and subsatellite magnetometer field differences and the solar wind plasma density. There is no correlation between solar wind velocity and perturbations in remanent field components. This correlation pattern is similar to that of Apollo 12 data in Figure 2.

Fig. 4

This correlation between the field perturbations and plasma density seen in the Apollo 12 and 16 data can be used to calculate the remanent field scale lengths at these sites. In Figure 5 we show the radial magnetic field difference

Fig. 5

ΔB_x calculated from Apollo 12 and Explorer 35 data and the corresponding field calculated from the field diffusion model using the solar wind density measured by the Apollo 12 solar wind spectrometer. The scale size L of the field is iteratively adjusted until the function f(n,L) multiplied by the steady field component best fits the measurements. Radial component data measured in the magnetosheath do not correlate with the theory as well as data measured in the solar wind. Other data sets show similar deviation from the diffusion model for short periods of time. We attribute this behavior to solar wind dynamic pressure, plasma thermal, and frequency dependent effects not incorporated in the field diffusion theory. The corresponding tangential field change and diffusion model field are in close agreement. This correlation is better shown in Figure 6 where the measured field difference is plotted on the ordinate and the field calculated from the diffusion model is plotted on the abscissa. With perfect agreement between measured field and theory the data would fit the straight line shown in the figure. The correlation between the measured and calculated fields was maximized to a value of 0.89 by using two remanent fields, each characterized by a different magnitude and scale size. In the analysis shown in Figures 5 and 6, a large magnitude 33 gamma field of scale size 18.5 km is superimposed on a 4.6 gamma field of scale size 100 km.

Fig.

The Apollo 15 measured and calculated remanent field changes are shown in Figure 7. There is very little correlation between these two fields, confirming our previous conclusions based only on surface field and plasma data in Figure 3.

Fig.

The Apollo 16 data in Figure 8 show a good correlation between the measured and calculated field changes. Correlation of the radial and tangential measured remanent field changes with the calculated field changes are 0.82 and 0.74 respectively using a 5.7 km, 187 gamma field superimposed upon a 100 km, 5.7 gamma field.

Fig.

Results of the remanent field analyses discussed above are summarized in Figure 9. Remanent field change tangential to the surface at the Apollo 12, 15, and 16 landing sites is plotted as a function of the measured solar wind density. Larger data sets were used here than in previous analyses. For each site the averaged data is compared to the diffusion model calculations with three different scale lengths for the local field values. It is apparent that the Apollo 12 and 16 analyses are relatively sensitive to the model scale lengths.

Fig. 9

CRUSTAL MAGNETIC FIELD RESULTS AND CONCLUSIONS

From remanent field-plasma interaction analyses, we have estimated the local field scale lengths at the Apollo 12 and 16 sites. An important comparison can be made between these results, the portable magnetometer traverse measurements, and the subsatellite magnetic maps.

The 5.7 km scale size calculated for remanence in the Descarte region is in agreement with measurements of the lunar portable magnetometer over a 7 km traverse by astronauts Young and Duke. At three different measurement sites along a 1.5 km traverse, the local field was directed uniformly down and to the northwest. Measurements over a 7 km traverse oriented orthogonally to the 1.5 km traverse, revealed a local field directed up and southwest at one extreme and down and southwest at the other extreme. These measurements of the lunar portable magnetometer confirm the remanence scale size determined from field diffusion analysis.

Anderson et al. (1972) used the charged particle experiment on the Apollo 15 and 16 subsatellites to measure crustal remanent fields by observing the electrons reflected by the fields back to the satellite. The magnetic maps of the lunar surface generated by this technique have a spatial resolution of 7.6 km. These maps are in excellent agreement with our surface measurements (R. P. Lin, private communication 1978). Each field measurement depends upon

the instantaneous interplanetary field direction and the subsatellite location so that the maps do not have continuous coverage. Within 15 km of the Apollo 12 landing site the particle reflection experiment measured fields from 10 to 100 gammas which are in accord with the surface measurement of 38 gammas over a scale length of 18.5 km.

There is no direct electron reflection measurement from the Apollo 15 site location. However, in five map resolution elements (7.5 km square) near the site, the measured field is zero within experimental error. At one adjacent map element the field is 0.3 gammas. Again these results agree with the Apollo magnetometer measurement of 3.4 ± 2.9 gammas.

The electron reflection field measurement nearest the Apollo 16 site was for an area 15 km away with a field magnitude of 2.0 gammas. Because the Apollo field scale size is 5.7 km we do not expect the remanent field 15 km distant to be characteristic of the Apollo site. Within fifteen map resolution elements (100 km) of the Apollo 16 site the electron reflection technique measures fields greater than 1000 gammas. These comparisons of surface and orbital magnetic measurements are the first comprehensive tie between high spatial resolution, limited coverage surface measurements and the lower resolution, extended coverage maps obtained with the subsatellite experiment.

Investigation of the remanent field-solar wind interaction has permitted calculation of the characteristic scale of magnetization in the Apollo 12 vicinity to be 19 km, and in the Apollo 16 vicinity to be 6 km. These results have been shown to be in agreement with the astronaut traverse magnetic measurements at Apollo 14 and 16, the Lunokhod 2 traverse magnetic measurements, and the surface magnetic maps from the particles and fields subsatellite experiments. We conclude from information provided by all of these experiments that remanent fields with magnitude up to several hundred gammas, which are found over much of the lunar surface, are characterized by spatial variations

as small as a few kilometers. As shown schematically in Figure 10, this conclusion implies that the magnetized sources for the remanent fields are more or less randomly distributed in the lunar crust with a characteristic scale of a few kilometers. This magnetized material may be broken from and reoriented with respect to larger scale uniformly magnetized regions. This model would result in remanent fields of scale length 5 to 10 km and magnitude $\sim$ 100 gammas near the surface in accord with measurements of lunar surface magnetometers, and weaker fields of scale length 50-100 km and magnitude $\sim$ 0.1 gammas at 100 km altitude in accord with measurements of subsatellite instruments. A simple calculation of fields associated with the remanence measured in returned lunar samples demonstrates the validity of this model of crustal magnetization. A disk uniformly magnetized along its axis at 4×10^{-5} emu/gm, with a radius 50 km and thickness 10 km representing a large scale magnetized region of the crust, has an axial field at its top surface of about 4 gammas and a field 100 km above the surface at subsatellite altitude of 0.4 gammas. A spherical piece of this disk of radius 5 km, representing impact debris responsible for the small scale field, has a magnetic field at its surface of 100 gammas, however at a distance of 100 km the field is only 0.01 gammas. This model is consistent with present knowledge of the lunar crustal evolution, however it is not unique and other models may also be consistent with the magnetic data.

We hypothesize that large regions of the lunar crust 50 to 100 km in extent and tens of kilometers thick were magnetized early in lunar history; perhaps as early as 4.3 to 4.4 billion years (b.y.) ago (Toksöz and Johnson, 1974) as the crust cooled through the iron Curie temperature. The mechanism for this magnetization is still unknown, however available data strongly indicate a nearly random, local mechanism rather than a uniform, global magnetizing process (Dyal et al., 1977; Srnka, 1977; and Gold and Soter, 1976).

Excavation of large mare basins in the solidified crust between 4.4 and 3.9 b.y. ago, removed much of the magnetized material from the basins. The scattered magnetized material from basin formation and from the intense bombardment epoch 4 b.y. ago left a layer of small scale, randomly oriented magnetized debris over much of the lunar surface. Mare basin flooding, between 3.9 and 3.2 b.y. ago, heated the basin floors above the Curie temperature erasing most of the remanent magnetization beneath the basins. Subsequent alteration of crustal magnetization has probably been minor. This scenario is consistent with what is known of crustal evolution, the results of orbital magnetic experiments, and our investigation of the remanent magnetic field scale sizes at the lunar surface.

Acknowledgments--The authors are grateful to G. Lathrop of Computer Sciences Corporation for programming support and to Marion Legg and her colleagues at Diversified Computer Applications for analysis of voluminous data. Solar wind spectrometer data for this analysis was kindly provided by Dr. Douglas Clay. We also acknowledge Dr. Curtis Parkin for his diligent work in this lunar research project. We especially thank Dr. Robert Lin for discussions of recent unpublished results from the electron reflection experiment. Research support for W.D.D. under NASA grant NSG-2082 is gratefully acknowledged.

REFERENCES

Anderson K.A., Chase L.M., Lin R.P., McCoy J.E., and McGuire R.E. (1972) Solar-Wind and Interplanetary Electron Measurements on the Apollo 15 Subsatellite. J. Geophys. Res. 77, 4611-4626.

Barnes A., Cassen P., Mihalov J.D., and Eviator A. (1971) Permanent Lunar Surface Magnetism and Its Deflection of the Solar Wind. Science 171, 716-718.

Clay D.R., Goldstein B.E., Neugebauer M., and Snyder C.W. (1972) Solar Wind Spectrometer Experiment. In Apollo 15 Prelim. Sci. Rep., NASA SP-289, p. 10-1 to 10-7.

Clay D.R., Goldstein, B.E., Neugebauer, M., and Snyder C.W. (1975) Lunar Surface Solar Wind Observations at the Apollo 12 and Apollo 15 Sites, J. Geophys. Res. 80, 1751-1760.

Coleman P.J., Jr., Schubert G., Russell C.T., and Sharp L.R. (1972) The Particles and Fields Subsatellite Magnetometer Experiment. In Apollo 15 Prelim. Sci. Rep., NASA SP-289, p. 22-1 to 22-9.

Dolginov Sh. Sh., Yeroshenko Ye. G., Sharova V.A., Vnuchkova T.A., Vanyan L.L., Okulessky B.A., and Bazilevsky A.T. (1976) Study of Magnetic Field, Rock Magnetization and Lunar Electrical Conductivity in the Bay LeMonnier, The Moon 15, 3-14.

Dolginov Sh. Sh., Yeroshenko Ye. G., Zhuzgov L.N., Sharova V.A., Vnuchkov G.A., Okulessky B.A., and Bazilevsky A.T. (1977) Magnetic Field in LeMonnier Bay according to data of Lunokhod 2. NASA SP-370, 433-441.

Dyal P. and Gordon D.I. (1973) Lunar Surface Magnetometers. IEEE Transactions on Magnetics, MAG-9, No. 3, 226-231.

Dyal P., Parkin C.W., and Sonett C.P. (1970) Apollo 12 Magnetometer: Measurement of a Steady Magnetic Field on the Surface of the Moon. Science 169, 762-764.

Dyal P., Parkin C.W., Snyder C.W., and Clay D.R. (1972) Measurements of Lunar Magnetic Field Interaction with the Solar Wind. Nature 236, 381-385.

Dyal P., Parkin C.W., and Daily W.D. (1977) Global lunar conductivity and thermoelectric origin of remanent magnetism. Proc. Lunar Sci. Conf. 8th., p. 767-783.

Gold T. and Soter S. (1976) Cometary Impact and the Magnetization of the Moon. Planet. Space Sci. 24, 45-54.

Jackson J.D. (1962) Classical Electrodynamics, pp. 162-164. John Wiley and Sons, New York.

Nagata T., Fisher R.M., Schwerer F.C., Fuller M.D., and Dunn J.R. (1972) Rock Magnetism of Apollo 14 and 15 Materials. Proc. Lunar Sci. Conf. 3rd., p. 2423-2447.

Neugebauer M., Snyder C.W., Clay D.R., and Goldstein B.E. (1972) Solar Wind Observations on the Lunar Surface with the Apollo 12 Alsep. Planet. Space Sci. 20, 1577-1591.

Runcorn S.K., Collinson D.W., O'Reilly W., Stephenson A., Greenwood N.N., and Battey M.H. (1970) Magnetic Properties of Lunar Samples. Science 167, 697-699.

Siscoe G.L., and Goldstein B. (1973) Solar Wind Interaction with Lunar Magnetic Fields. J. Geophys. Res. 78, 6741-6748.

Sonett C.P. and Mihalov J.D. (1972) Lunar Fossil Magnetism and Perturbations of the Solar Wind. J. Geophys. Res. 77, 588-603.

Sonett C.P., Colburn D.S., Currie R.G., and Mihalov J.D. (1967) The Geomagnetic Tail: Topology, Reconnection and Interaction with the Moon. In Physics of the Magnetosphere (Editors R.L. Carovillano, J.F. McClay, and H.R. Radoski), pp. 461-484. D. Reidell, Dordrecht, Holland.

Srnka L.J. (1977) Spontaneous magnetic field generation in hypervelocity impacts. Proc. Lunar Sci. Conf. 8th., p. 785-792.

Strangway D.W., Gose W.A., Pearce G.W., and Carnes, J.G. (1973) Magnetism and The Early History of the Moon. J. Appl. Phys., 1178.

Toksöz M.N. and Johnson D.H. (1974) The Evolution of the Moon. Icarus 21, 389-414.

Vanyan L.L. (1977) The Interaction of the Solar Wind with Lunar Magnetic Anomalies. The Moon 16, 321-324.

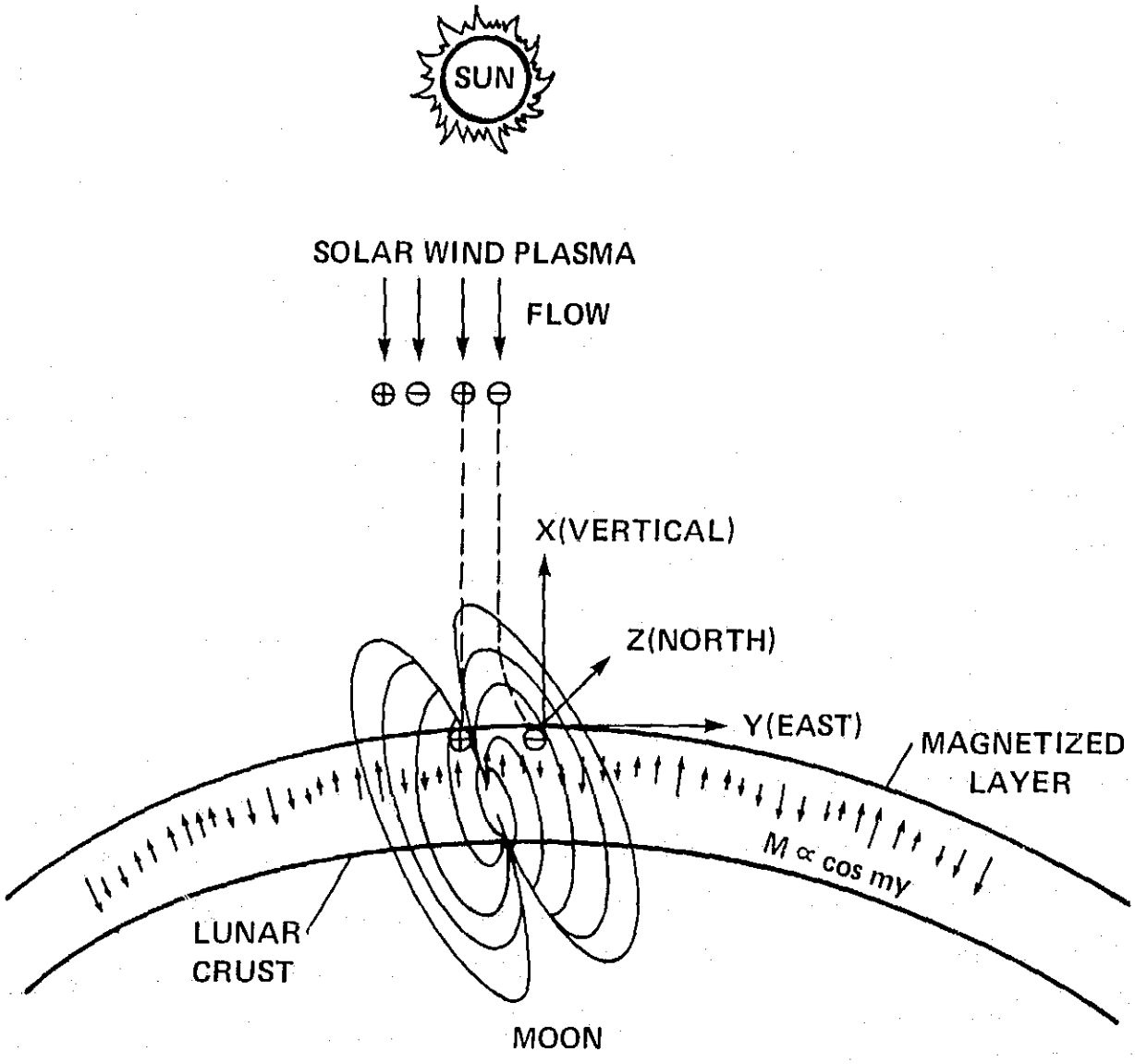

Figure 1 - Schematic representation of the remanent field-solar wind interaction. Magnetic fields near the lunar surface are produced by natural magnetic remanence in the crust. The neutral solar plasma impinges on the lunar surface with little change in its flow due to interaction with these local fields. The orthogonal coordinate system used in the analysis is also shown.

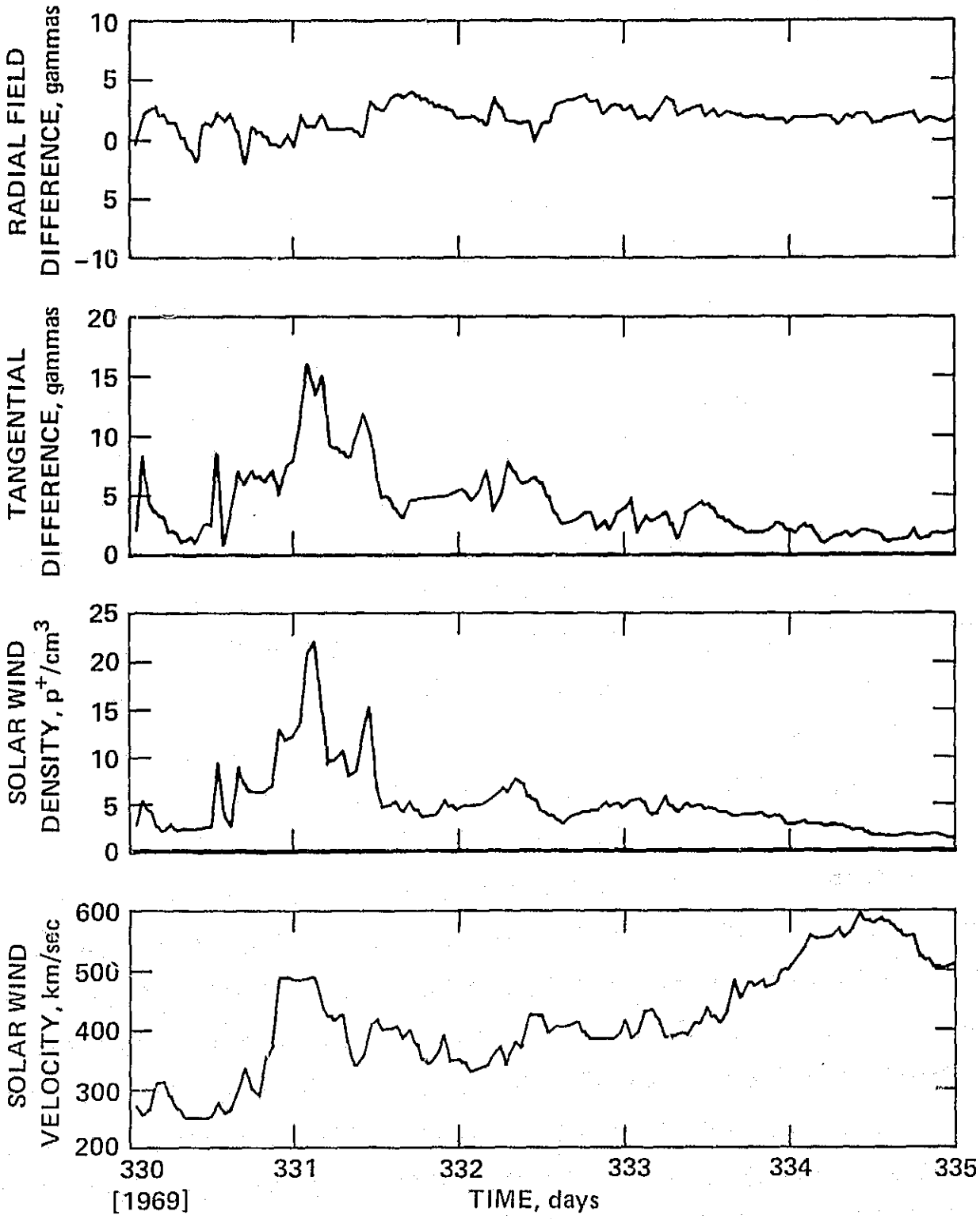

Figure 2 - Apollo 12 magnetometer and plasma one hour average data as a function of time for 5 days of the first post deployment lunation. The radial field difference is the x axis component as shown in Figure 1 and the tangential difference is the horizontal component at the site. The field differences are obtained by subtracting orbiting Explorer 35 magnetometer data from surface magnetometer data. This data is typical of that from many subsequent lunations.

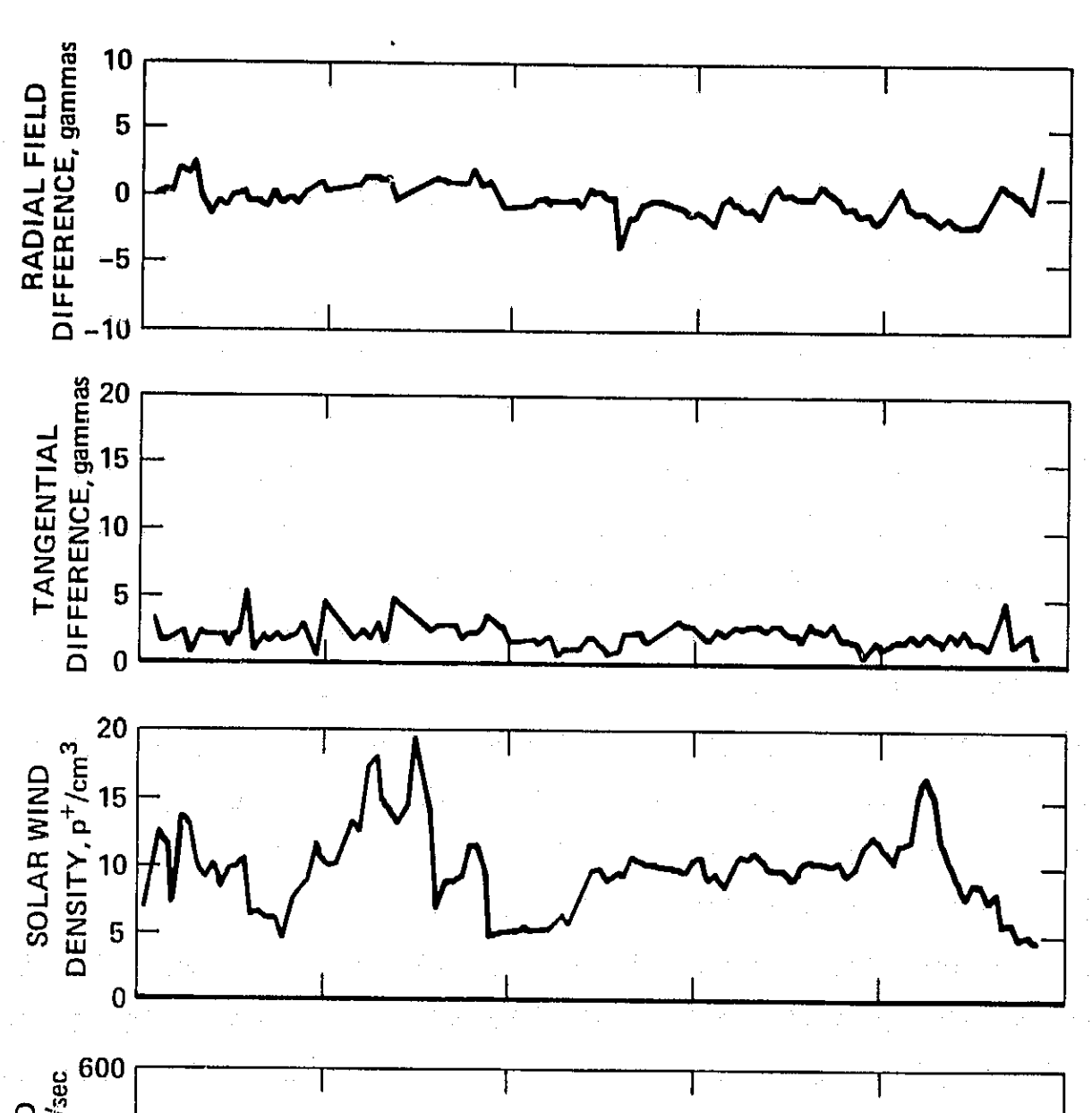

Figure 3 - Apollo 15 magnetometer and plasma one hour average data as a function of time for 5 days of the second post deployment lunation. The field differences are obtained by subtracting the orbiting Apollo 15 subsatellite magnetometer data from the surface magnetometer data.

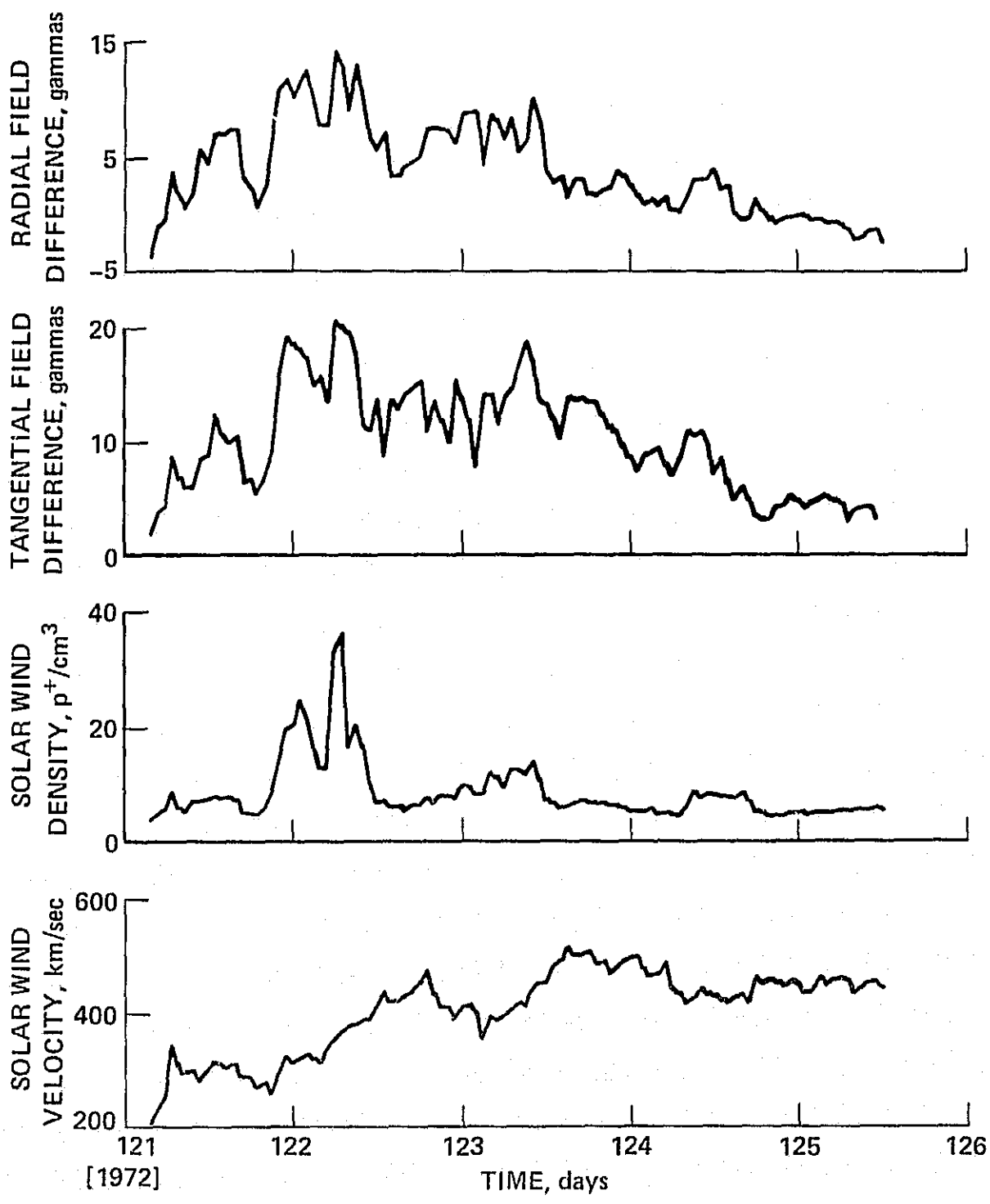

Figure 4 - Simultaneous Apollo 16 magnetometer and Apollo 15 plasma one hour average data as a function of time for 5 days of the first Apollo 16 post deployment lunation. The field differences are obtained by subtracting the orbiting Apollo 16 subsatellite magnetometer data from the surface magnetometer data.

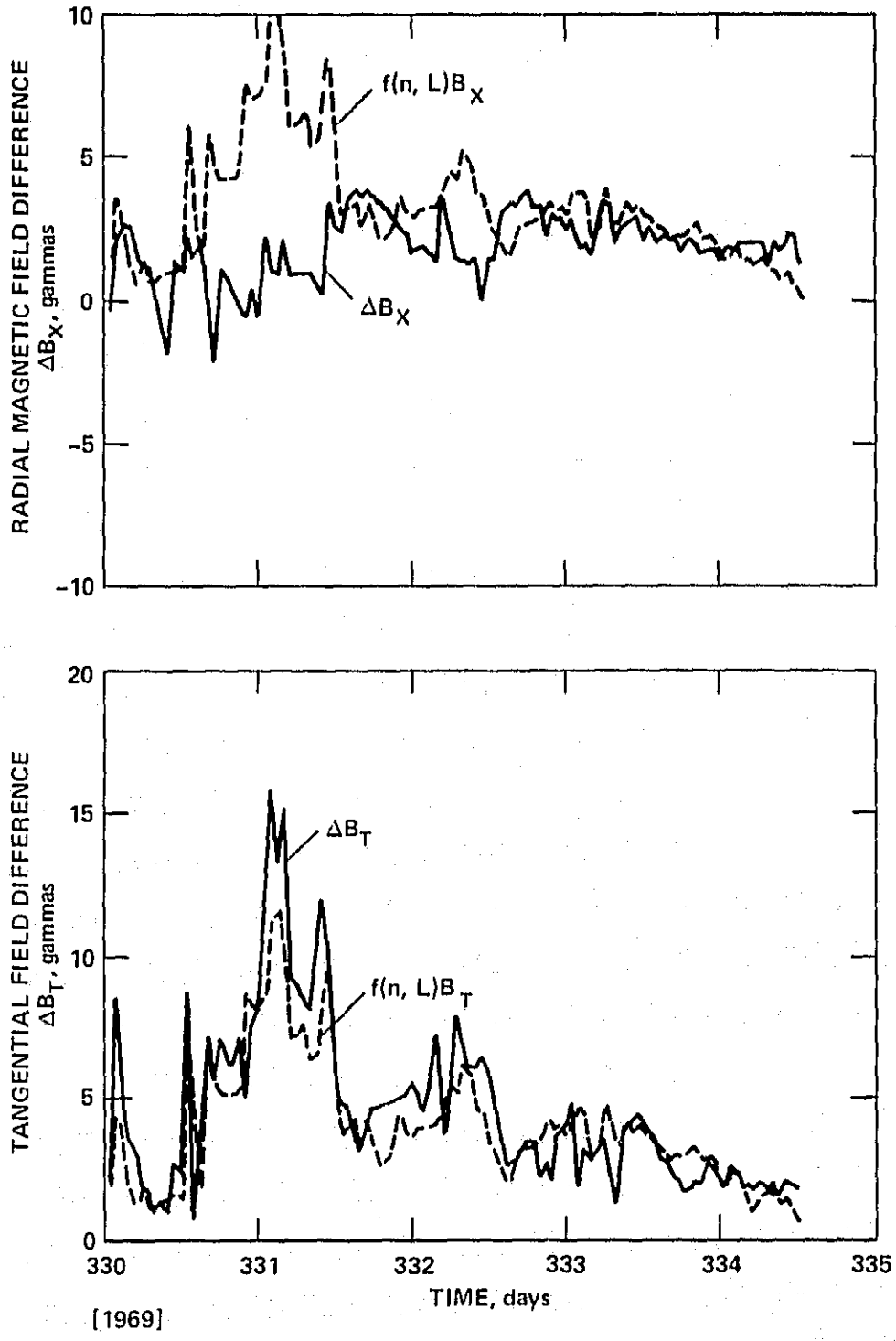

Figure 5 - Radial and tangential field differences of Apollo 12 surface and Explorer 35 orbital magnetometer data compared to the corresponding radial and tangential fields $f(n,L)\underset{\sim}{B}_R$ calculated using the field-plasma diffusion theory. One hour average data are used in this analysis.

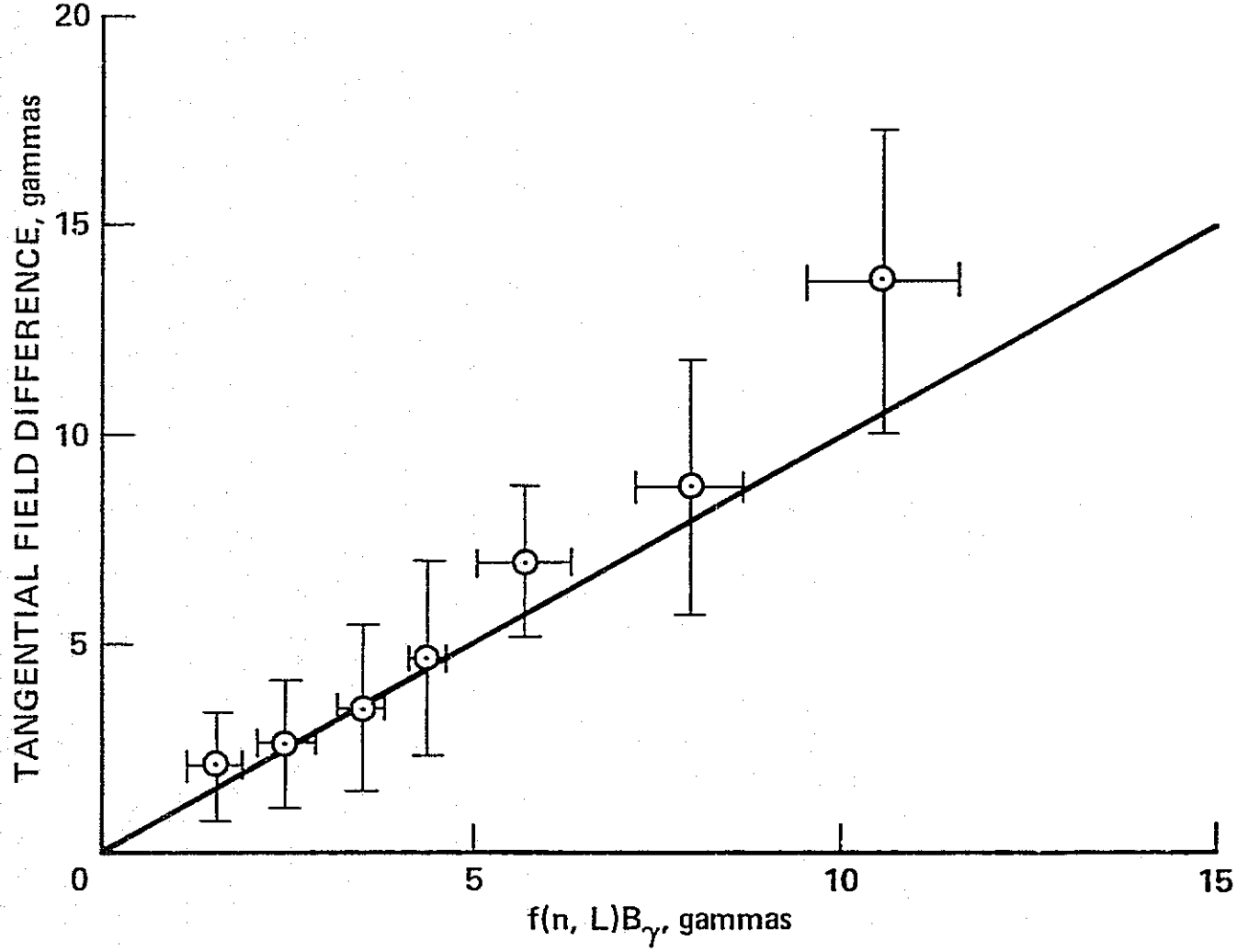

Figure 6 – Correlation plot of the tangential field difference between the Apollo 12 surface and Explorer 35 orbital magnetometer data and the corresponding tangential component of the field from B_{cR} calculated using the field-plasma diffusion theory. The two remanent field scale sizes for L are 18.5 km and 100 km respectively for the 33 gamma and 4.6 gamma fields. The straight line of slope 1 is indicative of perfect correlation and is compared to the averages of the one hour averaged measurements. Error bars on the verticle axis represent 1.5 standard deviations.

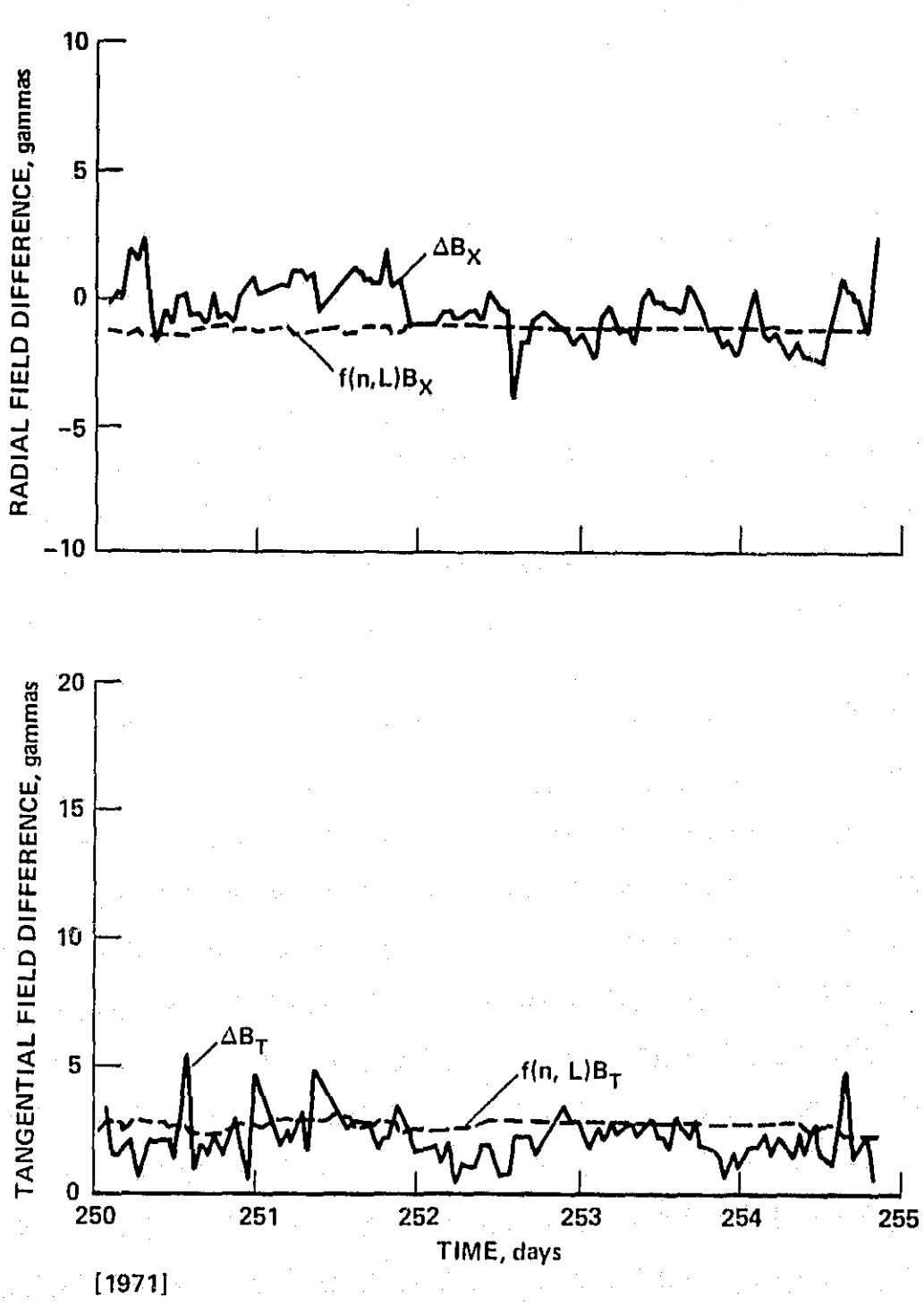

Figure 7 - Radial and tangential field differences of Apollo 15 surface and subsatellite magnetometer data compared to the corresponding radial and tangential fields $f(n,L)B_{R}$ calculated using the field-plasma diffusion theory. One hour average data are used in this analysis.

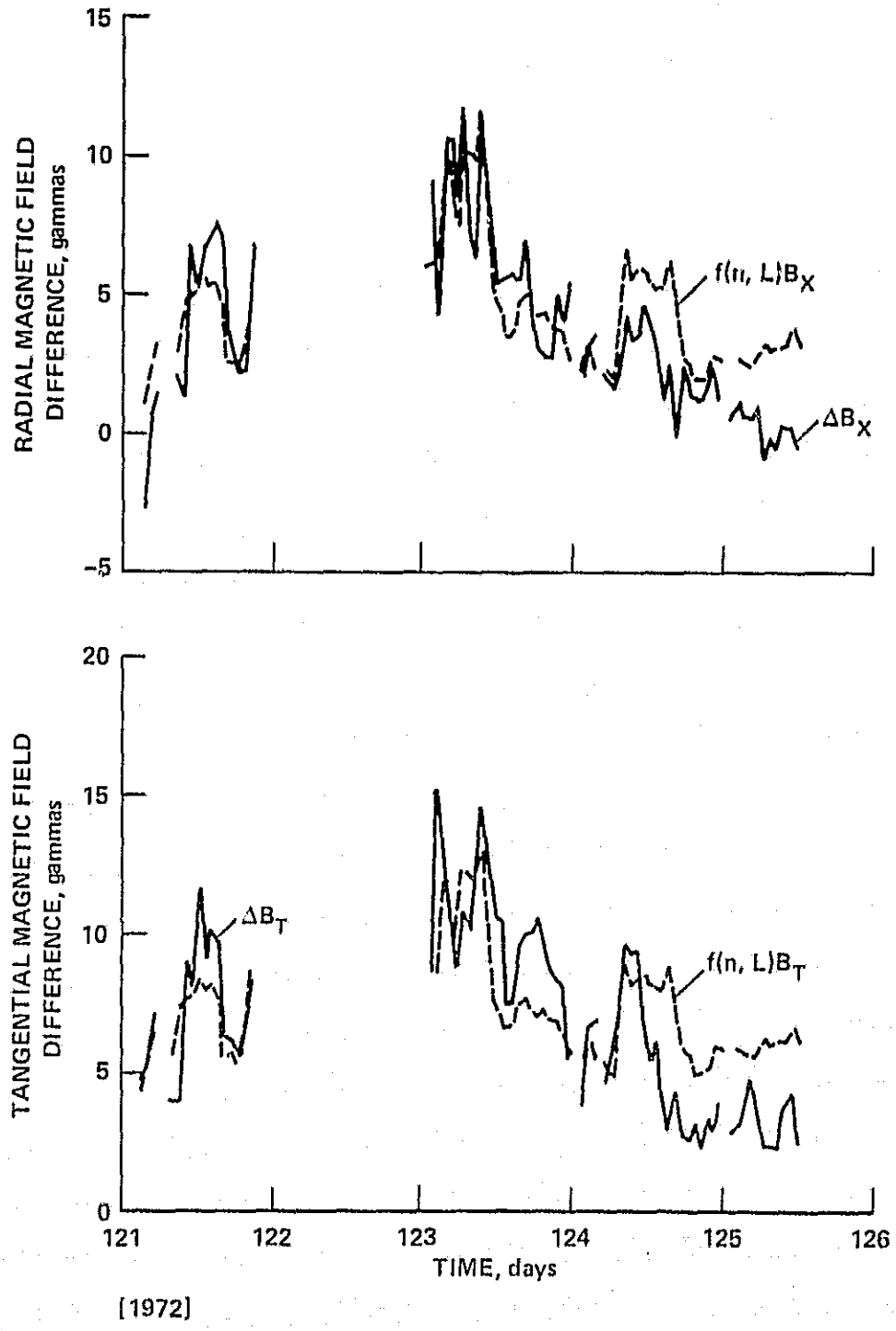

Figure 8 - Radial and tangential field differences of Apollo 16 surface and subsatellite magnetometer data are compared to the corresponding tangential component of the field $f(n,L)B_{R}$ calculated using the field-plasma diffusion theory. One hour average data are used in this analysis.

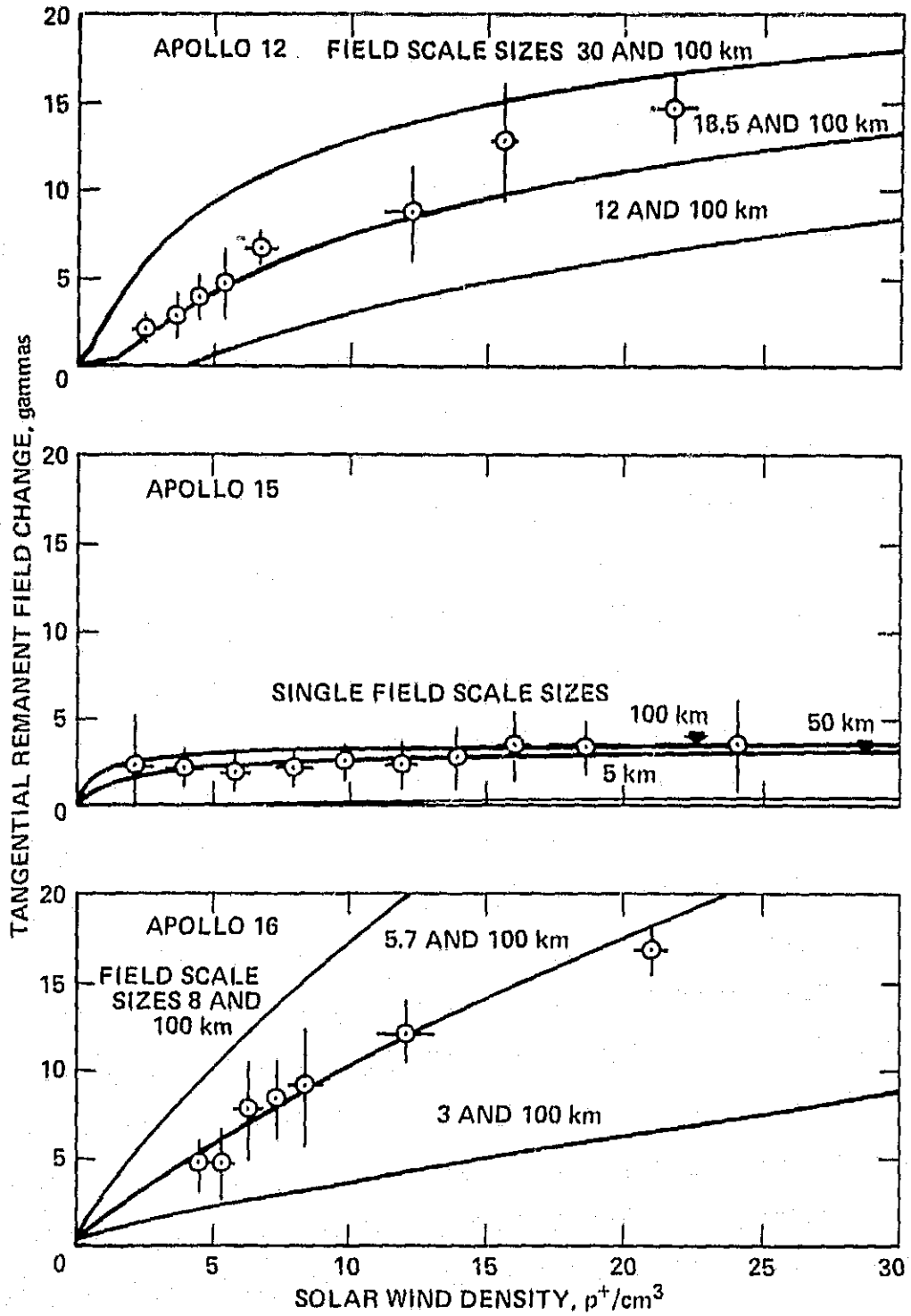

Figure 9 - The remanent magnetic field change tangential to the surface at Apollo 12, 15, and 16 landing sites plotted as a function of the solar wind plasma density measured at the lunar surface. The averaged data for each site are compared to 3 different models of the lunar remanent magnetic field. For the Apollo 12 models a small scale field of 33 gammas is superimposed on a 4.6 gamma 100 km scale field. The Apollo 15 models are a 4 gamma field of scale 5, 50, and 100 km. The Apollo 16 models are a small scale 146 gamma field superimposed on a 100 km scale, 1 gamma field.

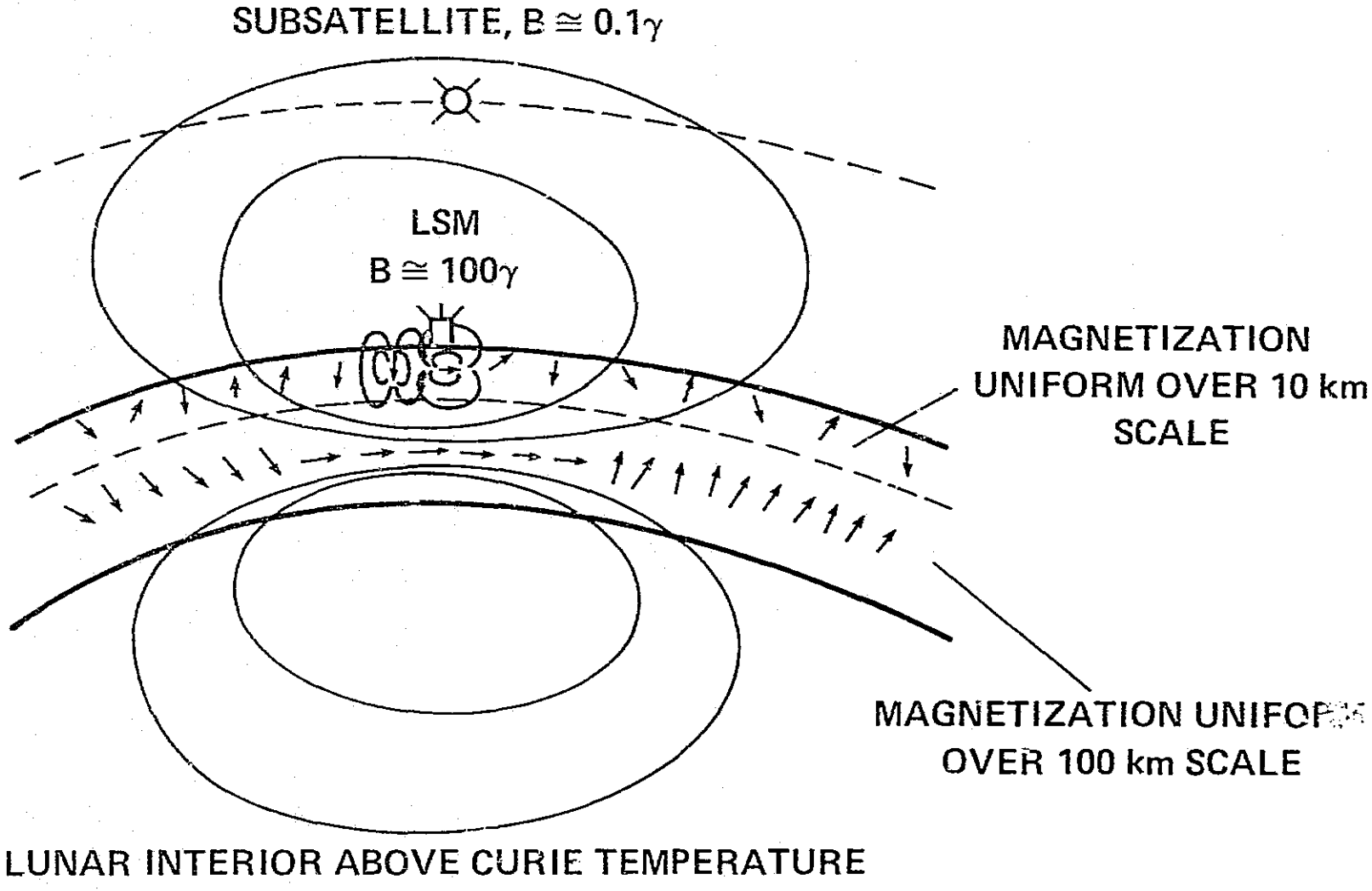

Figure 10 - Schematic model of the magnetized lunar crust is shown along with the surface and orbital instruments used in this diffusion model analysis. The magnetic remanence distribution illustrated here is consistent with the large scale magnetic features mapped by the Subsatellite Particles and Fields Experiments and the small scale magnetic features as deduced from analyses in this study.